RSC Advances

PAPER

View Article Online
View Journal | View Issue

Cite this: *RSC Adv.*, 2020, **10**, 28872

Hybrid approach to obtain high-quality $BaMO_3$ perovskite nanocrystals†

Natalia Chamorro,[ab] Jordi Martínez-Esaín,‡[ab] Teresa Puig,[b] Xavier Obradors,[b] Josep Ros,[a] Ramón Yáñez[a] and Susagna Ricart*[b]

A novel hybrid solvothermal approach for perovskite nanocrystal formation *via* accurate control of the hydrolytic process is reported. This new synthetic methodology sets a whole general route to successfully tune the sizes of high-quality $BaMO_3$ (M = Ti^{4+}, Zr^{4+}, and Hf^{4+}) perovskite nanocrystals. Purely cubic-phase nanocrystals (stable in alcohol media) were obtained using controlled water amounts, combining the well-known aqueous sol–gel process with the classic solvothermal method. Exhaustive optimizations revealed feasibility of a fast (1 hour) and reproducible synthesis with small variations in the crystal size or agglomeration parameters. The study also reveals water content as the pivotal factor to achieve this wide range of sizes through a controlled hydrolytic step. Finally, the study of the hydrolytic process made it possible to shed some light on mechanistic insights of this synthetic route.

Received 29th April 2020
Accepted 21st July 2020

DOI: 10.1039/d0ra03861j

rsc.li/rsc-advances

Introduction

Nowadays, the search for a fast, cheap, reproducible and robust approach to synthesize oxide nanocrystals (NCs) still attracts strong attention among researchers. This high interest derives from their wide range of applications in electronics,[1] medicine,[2,3] catalysis,[4,5] energy storage[6,7] and sensing.[8] Among metal oxide NCs, the perovskite family has gained attention due to its stability under high-temperature treatments and its emergent applications.[9–11] Although, $BaTiO_3$ NCs have been extensively studied,[12–15] the achievement of $BaZrO_3$ and $BaHfO_3$ NCs continues to be an entangled process, in which researchers keep finding difficulties to obtain small-size, crystalline NCs, stable in colloidal suspensions without agglomeration.[16–18]

Although the applicability of these systems is clear and well-known, the synthesis of this family of perovskites still entails many limitations to obtain stable, homogeneous and high-quality NCs. Our main goal is to find alternative methods for these intricate perovskite NCs using the current background researches in the field. Two main strategies are highlighted: (i) non-aqueous solvothermal treatments and/or (ii) sol–gel aqueous processes. Although the hydrolytic mechanism of the aqueous sol–gel procedure is well-known,[19–21] this methodology is usually avoided because the fast hydrolysis promotes formation of non-homogeneous systems; this requires a posterior calcination treatment, reducing the final NC stability in solution.[12,22] On the other hand, non-aqueous approaches[23–27] have risen up during last decades due to several advantages such as high crystallinity, controlled crystal growth and homogeneous NC dispersions.[28,29] However, this methodology shows two main drawbacks: long reactions times and the need to use high temperatures during the process.[12,17,18] We aimed to go further by trying to control the hydrolytic step with different water proportions applying same conditions as in the "non-aqueous" methodology. This approach aims to merge the advantages of both routes (*i.e.*, sol–gel and solvothermal) of perovskite synthesis in one that combines short reaction times, high crystallinity and long stability of the NCs.

Herein, we not only report a suitable synthetic methodology for a group of perovskite NCs ($BaMO_3$) but also a general route that allows accurate size control of high-quality NC systems. This new proposed synthetic procedure has been tested for three tetravalent cations (Ti^{4+}, Zr^{4+} and Hf^{4+}), being the first time that the same methodology can be applied to this perovskite family, obtaining comparable quality NCs. This novel approach allows to fine-tune the NC size and an excellent uniformity of NCs dispersion, with promising applications in emergent energetic devices. The present work conducted by our group showed the possibility to combine $BaZrO_3$ and $BaHfO_3$ NCs with $YBa_2Cu_3O_7$ (YBCO) type II superconductors, to enhance the superconducting properties, unravelling a novel pathway in electronic materials science and bestowing a crucial breakthrough for the implementation of NCs to act as pinning centres.[30–32] Thus, we present here a novel hybrid method (*i.e.*,

[a]*Departament de Química, Universitat Autònoma de Barcelona, 08193 Bellaterra, Spain*

[b]*Institut de Ciència de Materials de Barcelona (ICMAB-CSIC), 08193 Bellaterra, Spain. E-mail: ricart@icmab.es*

† Electronic supplementary information (ESI) available. See DOI: 10.1039/d0ra03861j

‡ Present address: Catalan Institute of Nanoscience and Nanotechnology (ICN2), CSIC and The Barcelona Institute of Science and Technology, Campus UAB, Bellaterra, 08193 Barcelona, Spain.

built from the classical approaches) to produce high-quality perovskite NCs and enhance the current applicability portfolio.

Experimental methods

Materials

The following chemicals were used without further purification. Zirconium(IV) *n*-butoxide solution 80 wt% in *n*-butanol, hafnium(IV) *n*-butoxide 99%, titanium(IV) *n*-butoxide, triethylene glycol (TEG 99%), barium hydroxide octahydrate ≥98% and ammonium hydroxide solution 30% v/v were purchased from Sigma Aldrich. Ethanol absolute was purchased from Scharlau.

Nanocrystal synthesis

In a standard procedure, 1.24 mL (2.8 mmol) of $Zr(OC_4H_9)_4$ or 2.8 mmol of the desired *n*-butoxide precursor ($M = Ti^{4+}$, Zr^{4+} or Hf^{4+}) was added to 10 mL of absolute ethanol at room temperature under N_2 atmosphere and vigorous stirring for 5 min. Followed by the addition of barium hydroxide octahydrate, 1.104 g (3.5 mmol) until forming a homogeneous solution (10 min). Then, 6 mL of triethylene glycol (TEG, capping ligand) and 1 mL of NH_3 30% v/v solution (or instead the corresponding mmol of water detailed later in this work) were added under continuous stirring at room temperature resulting in a milky solution (5 min). The final suspension was transferred into a steel autoclave equipped with a Teflon-line and heated up at 180 °C under constant stirring for 1 hour and slowly cooled down to room temperature. The resulting orange-coloured suspension was washed as follows. Firstly 10 mL of ethyl acetate was added, sonicated during 10 min and then centrifuged at 10 000 rpm for 10 min. Then, supernatant was discarded and 10 mL of ethyl acetate : ethanol (4 : 1) were added, the mixture was sonicated until total dispersion of the pellet and later centrifuged at 10 000 rpm for 10 min (this washing procedure was repeated twice). In the final step, the pellet was dispersed into absolute ethanol. To ensure a homogeneous size distribution of the NCs an extra centrifugation of 10 min at 7000 rpm was performed, discarding the pellet and keeping the supernatant, with yield loss of 15–20% from the initial.

Microwave synthesis was performed following the same procedure as solvothermal reaction but replacing 1 mL of NH_3 30% v/v solution with 0.5 mL H_2O (added in the same step). After the mixing, the resulting milky solution was transferred to the MW Teflon and heated with a ramp of 36 °C min^{-1} until 180 °C for the $BaMO_3$ ($M = Zr^{4+}$, and Hf^{4+}) and 100 °C for the $BaTiO_3$, holding the corresponding final temperature for 5 min Afterwards, the same cleaning process as the solvothermal procedure was performed and finally dispersed into absolute ethanol.

Characterization

X-ray powder diffraction (XRD) samples were recorded by a Phillips XPert diffractometer equipped with a two circle diffractometers and Cu tube. Transmission electron microscopy (TEM) micrographs were obtained on a 120 kV JEOL 1210 TEM, Transmission Electron Microscopy (HRTEM) micrographs obtained on a 200 kV JEOL 2011 TEM. Dynamic (SPECS GmbH, Berlin, Germany) in ultra-high vacuum conditions (base pressure 4×10^{-10} mbar) with a monochromatic aluminium Kα X-ray source (1486.74 eV). Light scattering (DLS) was done using a Zetasizer Nano. XPS measurements were performed with a Phoibos 150 analyser. Micro-Raman measurements were performed in backscattering geometry at room temperature using the 5145 Å line of argon-ion laser with a XploRA PLUS Raman spectrometer from Horiba, attached to an Olympus microscope and equipped with CCD detector. To perform microwave reaction, a microwave advanced flexible synthesis platform (flexiwave) from milestone was used.

Results and discussion

The hybrid solvothermal method

According to our previous experience in metal oxide NC synthesis, we aimed to use a modified polyol route[33] and make it compatible with the $BaMO_3$ ($M = Ti^{4+}$, Zr^{4+} and Hf^{4+}) perovskite oxide NCs. The optimised procedure requires mixing 10 mL of ethanol and 6 mL of TEG to prevent the agglomeration or further precipitation.

The versatility of this approach is reflected by obtaining aggregation-free monodisperse $BaMO_3$ ($M = Ti^{4+}$, Zr^{4+} or Hf^{4+}) NCs (Fig. 1a–c, respectively) with a uniform size and shape, as corroborated by the histogram in Fig. S1.† The transmission electron microscopy (TEM) images and powder X-ray diffraction (XRD) reveals a square-like shape of the $BaZrO_3$ with a ~8 nm size while the two other perovskites (Ti^{4+} and Hf^{4+}) showed spherical shape with sizes of 8 and 7 nm respectively. These results are in close concordance with those calculated using the Scherrer equation (Table 1). Moreover, the resulting perovskites

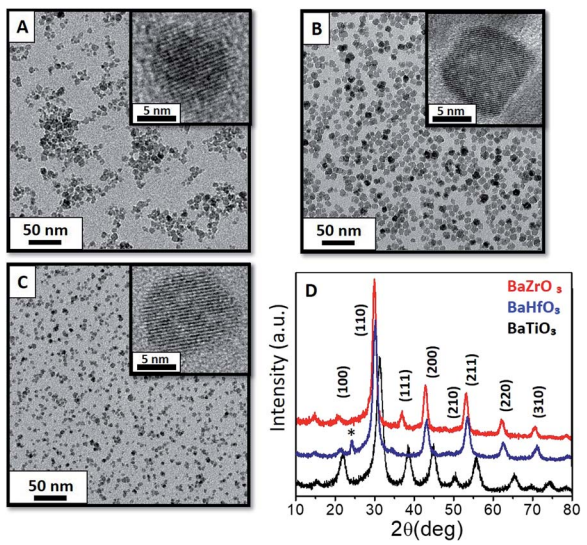

Fig. 1 TEM images of $BaTiO_3$ (a) $BaZrO_3$ (b) and $BaHfO_3$ (c) by using hybrid solvothermal reaction at 180 °C and 1 hour, showing their corresponding HRTEM. The index of Miller of the principal peaks by XRD (d) have been assigned into the diffractogram to confirm the cubic structure. On $BaHfO_3$ appears an * $BaCO_3$ peak suggesting a 5% of impurity on the pattern.

Table 1 Summary of average sizes (Scherrer and TEM) and morphology of the obtained perovskites NCs

NCs	Scherrer size (nm)	TEM size(nm)	Morphology
$BaTiO_3$	7.8	8.3 ± 1.4	Spherical
$BaZrO_3$	8.2	8.6 ± 1.5	Square-like
$BaHfO_3$	6.8	7.0 ± 1.2	Spherical

show high crystallinity, without the need of thermal treatments after the synthesis (Fig. 1d) contrarily to standard sol–gel procedures.

Many perovskite NCs from this family have been synthesised using stoichiometric amounts of Ba : M (1 : 1), even though the resulting NC systems are not homogeneous enough nor well dispersed.[34–36] Nonetheless, it has been demonstrated that the addition/excess of hydroxide compounds could lead to an increment on homogeneity and NC sizes, as well as, a better defined NCs shape.[37,38] We aimed to perform our hybrid solvothermal method in both conditions (*i.e.* stoichiometric and non-stochiometric Ba : Zr ratios) to study its effect to $BaZrO_3$ NCs. As shown in Fig. S2a,† the use of stoichiometric Ba : Zr ratio produced a non-homogeneous NC dispersion with agglomeration observed *via* TEM and corroborated with DLS (*i.e.* NC size one magnitude order higher than non-stoichiometric ones). However, both NC dispersions show the same cubic phase in XRD (Fig. S2c†), making us to postulate a surface effect on the stabilization of the NCs allowed with an excess of $Ba(OH)_2$.

As these NCs appear as good candidates for a wide range of material applications, assessing their stability and dispersion is mandatory. The DLS analysis revealed that the NCs remain well dispersed and stable in alcohols for 6 months, at concentration up to 80 mM for all cases. DLS analysis of the $BaTiO_3$, $BaZrO_3$ and $BaHfO_3$ NCs in EtOH, show that they are stable in solution at least 6 months, exhibiting constant sizes of 7–10 nm, in close agreement with the results obtained by TEM and XRD techniques (Fig. 2).

To study the crystal structure stability, the Goldschmidt tolerance factor (t) equation (eqn (1))[39,40] was reported as a powerful tool to predict the stability based only on the $BaMO_3$ perovskite compounds. This equation has a direct dependence on the ionic radii of each element ($BaMO_3$), where r_B is the ionic radius of Ba, r_M the ionic radius of (M = Ti^{4+}, Zr^{4+} or Hf^{4+}) and r_O the ionic radius of oxygen. To corroborate the stability of a cubic perovskite by tolerance factor the range of values should be between 0.8 and 1.05. In the case of M = Zr^{4+} and Hf^{4+}, a tolerance factor of $t = 1$ is obtained (Table 2), which is considered as the ideal cubic structure, where the ions are in a perfect cubic lattice.

$$t = \frac{(r_B + r_O)}{\sqrt{2}(r_M + r_O)} \quad (1)$$

Applying eqn (1) to the $BaTiO_3$, a value of $t > 1.05$ is obtained due to a smaller size of Ti^{4+} cations, this might cause a distortion on the lattice structure which could entail a transition from cubic phase to tetragonal, therefore showing a ferroelectric behaviour.

To verify the possibility of tetragonal phase, XRD diffraction could show some limitation since both, cubic and tetragonal phase, may coexist together. This would be observed by a split peak over 45° in 2θ in the XRD as an evidence of tetragonality. Although Fig. 1d shows an individual broad peak, the assignation cannot be fully attributed to cubic phase as a consequence of working at such reduced sizes (8 nm), which limits the XRD analysis.

To complete the study on the phase transition a complementary analysis using Raman spectroscopy was performed (Fig. S3†). The inactive bands present on paraelectric cubic phase (176, 270 and 520 cm^{-1}) become active on the transition to tetragonal phase[13,14,42,43] at 306 cm^{-1} (sharp peak) and 713 cm^{-1} with well-defined and high intensity peaks are the footprints to determine the tetragonally. $BaTiO_3$ NCs powder at room temperature was analysed, observing the absence of a sharp peak at 306 cm^{-1}, and a subtle broad peak on 713 cm^{-1} without good definition. The information extracted from this data suggests a non-dominant tetragonal phase on the NCs which leads to cubic perovskite postulation.

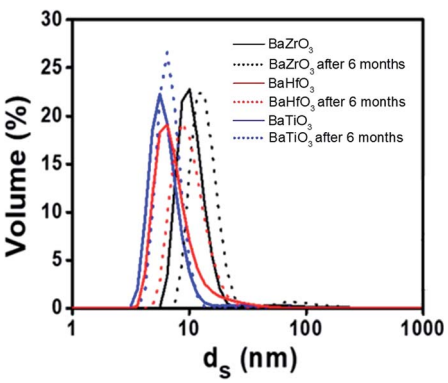

Fig. 2 A stability study by using DLS for monitoring the stability of the nanocrystals ($BaTiO_3$, $BaZrO_3$ and $BaHfO_3$ synthesised at 180 °C for 1 hour) from the moment of the synthesis to 6 month, all of them in ethanol media.

Time and temperature screening

Special attention was paid to the tuning of the NC synthesis. In particular, temperature and time are claimed to have a direct effect on the size, shape and crystallinity of the final colloidal dispersions.[44] By using solvothermal methodology, we are inducing a temperature and pressure (depending on the

Table 2 Overview of the radii from each element of the different perovskites.[41] Ionic radius of O^{2-} is 1.40 Å

Perovskites BMO_3	Ionic radius [Å]				Tolerance factor
	Cation X^{2+}		Cation M^{4+}		
$BaZrO_3$	Ba^{2+}	1.61	Zr^{4+}	0.72	1.00
$BaHfO_3$	Ba^{2+}	1.61	Hf^{4+}	0.71	1.00
$BaTiO_3$	Ba^{2+}	1.61	Ti^{4+}	0.61	1.06

precursors and solvent) which will trigger the nucleation of the crystals and a posterior growth of these nuclei to mature crystals. For this purpose, we performed a study modifying the temperature and time to observe the correlation of these parameters with the final NCs (*i.e.*, sizes, shape, crystallinity).

Firstly, the temperature was decreased from 180 to 100 °C for 1 hour, as it is observed in Fig. S4.† The lack of crystallinity in the cases of $BaZrO_3$ and $BaHfO_3$ at 100 °C is shown in the XRD pattern (Fig. S5†) with a non-defined cubic shape, which entails not enough temperature to induce the final crystals. However, $BaTiO_3$ shows a similar cubic pattern synthesised at both temperatures 100 and 180 °C (Fig. S4 and Table S1†). From this standpoint, Ti^{4+} precursor needs low temperatures (*i.e.*, 100 °C) suggesting a different growth rate compared with the other two, $BaZrO_3$ and $BaHfO_3$ (*i.e.*, 180 °C). This difference in growth conditions could be driven by a faster supersaturation point and different surface energy by using titanium instead of zirconium or hafnium precursors.[44] Although each metal has a different chemical and physical proprieties, it should be noted the close similarities between hafnium and zirconium, showing almost identical radii compared with titanium.[45,46]

Then, we held the temperature and modified the reaction time from 1 to 24 hours (Fig. S6†). It is observed that 1 hour is more than enough to synthesise the NCs, reducing the current growth times for $BaZrO_3$ and $BaHfO_3$ on solvothermal procedure from hours to just 1 hour (Fig. S7†). XRD pattern (Fig. S7 and Table S2†) did not reveal any evidence of difference on crystallinity or size (*i.e.*, *via* Scherrer equation) between the different reaction times. Consequently, it seems that the nucleation rate of the NCs is almost instantaneous once they are subjected to an adequate combination of pressure and temperature in the autoclave, without changing the morphology of the NCs. Therefore, 1 hour is enough for the NC formation, and keeping the reaction 24 hours at the same temperature did not affect the agglomeration of the NCs and even refute the possibility of the NCs to suffer grain growth caused by an Ostwald ripening.

It is well known that microwave is claimed to reduce reaction time in the synthesis of oxide NCs compared with the solvothermal ones.[16,24] However, in our case we were able to achieve shorter times in the solvothermal reactions without the need of microwave procedure. Even still, the reaction was checked by microwave methodology (Fig. S8 and Table S3†) at 180 °C ($BaZrO_3$ and $BaHfO_3$) and 100 °C ($BaTiO_3$) for 5 minutes, giving comparable NCs as in the autoclave. Moreover, a microwave profile of $BaZrO_3$ has been exposed in Fig. S8b,† the graph shows the variation of pressure and temperature as functions of time, showing a pressure incrementation over 15 bars and a reduction in reaction time from 1 hour in solvothermal route to 5 minutes by applying a microwave route. In consequence, both heating procedures are compatible with the hybrid solvothermal method without significant difference in crystallinity, homogeneity or sizes. These results seem to evidence that the solvothermal reaction is only required to raise the system to a desired temperature and pressure for minutes to achieve the final crystallisation, leaving the possibility to govern size and agglomeration parameters by the previous aqueous sol–gel step, thus a kinetic control over the NCs.

Tuning the NC size

Using the standard method for the synthesis of $BaZrO_3$, 1 mL of aqueous NH_3 at 30% v/v is necessary to obtain the final NCs solution. The role of ammonia in the reaction was not clear, due to its ability to act as a base or as a cationic stabiliser on the NC surface (*i.e.*, as ammonium cation stabilizing the system).[47] In order to understand the role of the ammonia and its influence in the final nanoscale system, X-ray photoelectron spectroscopy (XPS) was performed. In Fig. S9† can be demonstrated the absence of nitrogen compounds on the NC surface, meaning that ammonia or ammonium cations are not playing a stabilization role.

To evaluate the role of NH_3, we compared the NCs obtained using 0.7 mL of water or 1 mL NH_3 at 30% v/v (being 0.7 mL of water) as shown in Fig. S10.† Comparing TEM images and XRD results, we claim that there is not difference between the use of 1 mL ammonia 30% v/v or directly using its equivalent amount of water (0.7 mL of water). NCs form homogeneous dispersion as observed in the TEM images with square-like NCs, narrow size distributions and cubic phase (Fig. S10†). This evidence, in addition with the XPS analysis, suggest that ammonia did not play any additional role in our methodology, being just the amount of water coming from ammonia solution who govern the NC formation.

To demonstrate the specific role of the water, we used several quantities (from 0 mmol to 139 mmol) to test which is the pivotal role of the water in the system (Table 3). The most striking result emerging from this data is how an incrementation of water contain (0, 28, 55, 83, 111 and 139 mmol) produces a continuous increment in size from 4 to 31 nm (Fig. 3 and Table 3) comparing the sizes by TEM average and Scherrer equation.

Firstly, a test without adding water in the media using the standard protocol as before (180 °C and 1 hour in autoclave) evidences initial seed formation of NCs (Fig. 3a). XRD pattern showed a high presence of $BaCO_3$ as the main product (Fig. S12†), suggesting that the water amount in the $Ba(OH)_2 \cdot 8H_2O$ is not enough to initiate the nucleation process or the conditions are not still suitable to obtain desired final NCs.

Considering the other cases (*i.e.*, from 28 to 139 mmol of water), DLS analysis corroborates by TEM sizes showing an increment of hydrodynamic radii while the amount of water

Table 3 Summary of the NC sizes by using TEM average and Scherrer equation obtained at different amounts of water

H_2O amount	Scherrer size	TEM size
0 mmol	—	—
28 mmol	7.4 nm	7.0 ± 1.2 nm
55 mmol	11.8 nm	11.9 ± 1.8 nm
83 mmol	14.1 nm	14.7 ± 3.5 nm
111 mmol	25.0 nm	25.8 ± 7.5 nm
139 mmol	29.0 nm	32.6 ± 9.8 nm

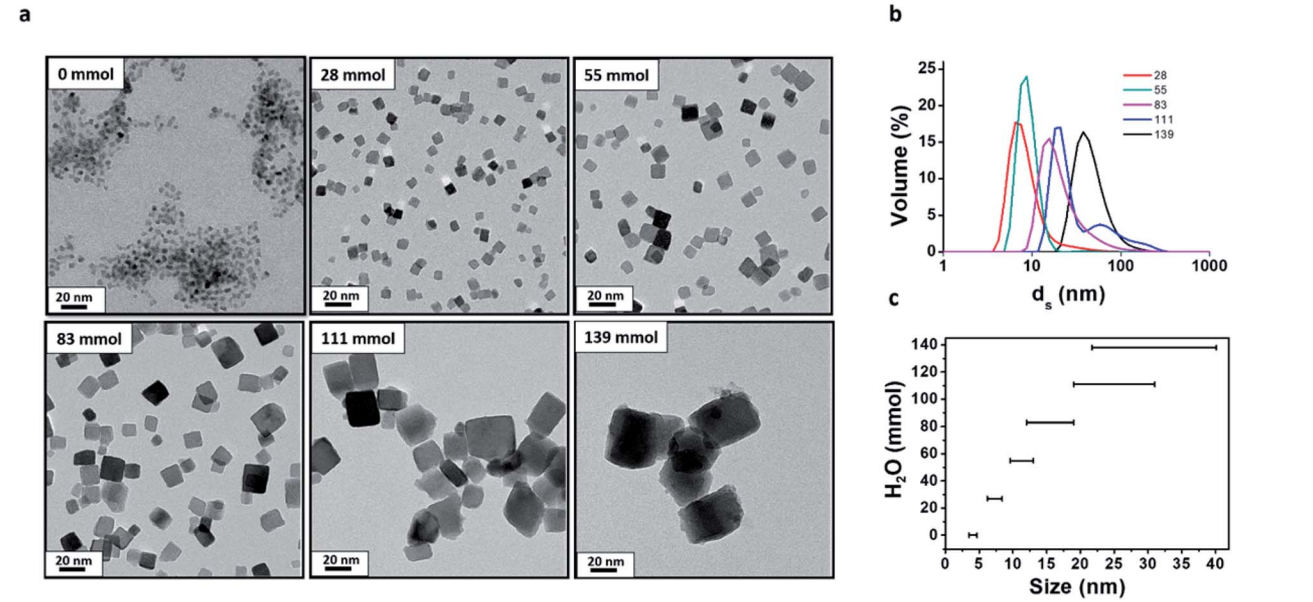

Fig. 3 (a) TEM images of $BaZrO_3$ NCs using different additional water amounts during the synthetic process (from 0 to 139 mmol). (b) DLS measurements of the different $BaZrO_3$ NCs at 28, 55, 83, 111 and 139 mmol of water (avoiding the ones at 0 mmol due to not fully formation NCs) and (c) the standard deviations of TEM histograms are showed to note the polydispersity when increasing water amounts.

increases, as well as, the stability of the NCs on the ethanol media (Fig. 3b). At this point, we realised that the effect of water is not only related to the increase of size but also in the polydispersity of final colloidal systems (Fig. 3c and S11†). Additionally, the standard deviation in TEM histograms increases with the size of the NCs. From a kinetic point of view, this effect could be explained by the hydrolysis step, if the nucleation process is increased without modifications on the thermodynamics, the system becomes polydisperse and with poor control on the stabilisation (*i.e.*, we are increasing the amount of water with the same amount of capping agent, TEG). Although NC size is tuned with the addition of different amounts of water, other properties are nearly similar in terms of shape, homogeneity and crystallinity. Concerning their crystalline structure, all NCs present a cubic structure with a $Pm\bar{3}m$ space group (Fig. S12†), in which Scherrer sizes match with the obtained *via* TEM and DLS (Table 3).

Mechanistic insights in the hybrid solvothermal method

To shed more light on this growing process we need to focus on the mechanistic insights of the reaction. If the NC size relies on the amount of water, the hydrolysis step should be the key factor in the control of the NC size, and hence, the behaviour of the metal cation against hydrolysis. Our starting precursors are alkoxides, and even though their chemical reactivity has been widely studied,[48,49] there is still noted a controversial aspect for knowing about the full mechanism reaction.[23,29]

As it is well known, the strategy of sol–gel is based on the hydrolysis and polycondensation steps (eqn (3)–(5)) and it has been extensible as the main step to synthesise oxide nanoparticles.[21,23,50,51] Herein by following this mechanism a sol–gel process is shown with a chemical reactivity tailored by the manipulation of the water amount. In an ethanol media, the stabilization and homogenisation of the alkoxide in the solvent is considered the first step to form the intermediate $M(OBu)_{4-x}(OEt)_x$ (eqn (2)). Alkoxides are extremely sensitive to water, so the addition of $Ba(OH)_2$ octahydrate plays a double role; (i) the addition of the binary cation for the perovskite structure and (ii) the source of –OH groups and water which will start the hydrolysis reaction (eqn (3)) and the formation of intermediate species based on a metal hydroxide bond $M(OH)_x(OBu)_{n-x}$. Polycondensations are promoted as it is described in eqn (4) and (5), forming a M–O–M framework, being a critical point for the further formation of final $BaMO_3$. The increase of –M–OH species in our reaction media is controlled with the addition of water, allowing the formation of large –M–O–M– chains (polycondensation), producing bigger NCs.

$$M(OBu)_4 + xEtOH \rightarrow M(OBu)_{4-x}(OEt)_x + xBuOH \quad (2)$$

$$M(OBu)_n + xH_2O \rightarrow M(OH)_x(OBu)_{n-x} + xBuOH \quad (3)$$

$$–M–OH + H–O–M \rightarrow –M–O–M– + H_2O \quad (4)$$

$$–M–OH + Bu–O–M \rightarrow –M–O–M– + BuOH \quad (5)$$

Simultaneously, this experiment was carried out with the other two different metal precursors Hf^{4+} and Ti^{4+} alkoxides, revealing important insights into the growth process of the NCs. The behaviour of $BaHfO_3$ is similar to $BaZrO_3$, the addition of water (28 and 111 mmols) increases the NC size from 4.6 ± 0.7 nm to 14.8 ± 3.4 nm respectively (Fig. 4a and b). However, the findings with $BaTiO_3$ do not support the previous research, showing a quite different behaviour not being the amount of water the one who governs the NCs tuning sizes. After adding 28 and 111 mmols of water, $BaTiO_3$ NCs do not show significant differences in size from 8.7 ± 2.6 and 9.2 ± 2.1 nm, respectively

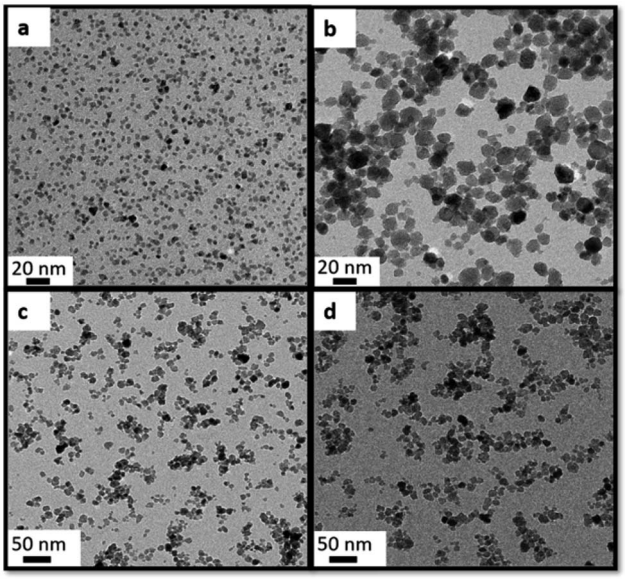

Fig. 4 Image by TEM of the synthesis of $BaHfO_3$ and $BaTiO_3$. In the case of (a) and (b) by adding 28 mmol and 111 mmol of water for synthesized $BaHfO_3$. On the case of (c) and (d) by adding 28 and 111 mmol of water for synthesized $BaTiO_3$.

(Fig. 4c and d). The experimental data taken from XRD (Fig. S13†) corroborates the TEM results.

A possible explanation for the difference of the titanium, can start from the behaviour of the alkoxide precursors on solution, as well as their tendency to polymerise. The formation of coordination polymers $[M(OR)_x]_y$ (where "y" is the degree of polymerisation) determines the final crystal formation. The degree of polymerisation has a direct dependency from the physical properties of the metals (i) the radius of the metal (Ti < Zr, Hf), (ii) the coordination number and (iii) the size of group R on the alkoxide. In our case, it seems that Hf and Zr are favourable to NC growth being the hydrolysis process that triggers the formation of –M–O–M– chains. While titanium cations exposed on the surface are less favourable to the NC growth, resulting on invariable NC size after water additions. Here, we need to consider the analogy between coordination chemistry and NC surface as the well-known covalent bond classification (CBC).[52,53] CBC is mainly based in the direct comparison between coordination chemistry and the surface of NCs, in which each metallic cation centre could be considered as a coordination complex. This hypothesis is supported by previous publications related to studies in coordination chemistry in which the authors found significant differences between the reactivity of titanium and zirconium alkoxides against hydrolysis and/or coordination.[45,50,54,55] Consequently, by controlling the hydrolysis step, different sizes of $BaZrO_3$ and $BaHfO_3$ NCs are produced. However, $BaTiO_3$ NCs show same sizes corroborating the different behaviour of these three elements from the same group of the periodic table.

Conclusions

In summary, we presented a dual-based synthetic approximation to obtain perovskite $BaMO_3$ NCs using a hybrid methodology. This novel strategy combines both aqueous sol–gel route and solvothermal reaction in a two-step process. As far as we know, this approach allows for the first time the use of the same methodology to obtain $BaTiO_3$, $BaZrO_3$ and $BaHfO_3$ NCs with high control of size, shape, reproducibility and stability.

In addition, by using this approximation, we evidenced the crucial role of water in the hydrolytic step, arising as a key parameter to tune the sizes of the final NCs. This allowed us to tune $BaZrO_3$ and $BaHfO_3$ size from 4 to 40 nm, and 4 to 15 nm respectively without deficiency of crystallinity and shape-defined appearance. In the other case, $BaTiO_3$ has a completely different behaviour, giving rise to constant 8–9 nm size NCs, independently of the water proportion.

Moreover, a complete study in a particular sized NCs show a stability of several months in polar solvents (*i.e.*, ethanol), being remarkable candidates for a full range of applications without taking care of the solution storage. This new outcome will open an interesting window for tuning NC sizes by the implementation of the described methodology and open a wide range of further applications.

Conflicts of interest

There are no conflicts to declare.

Acknowledgements

This work was supported by Spanish Ministry of Economy and Competitiveness through the "Severo Ochoa" Programme for Centres of Excellence in R&D (SEV-2015-0496), CONSOLIDER Excellence Network (MAT2015-68994-REDC), COACH-SUPENERGY project (MAT2014-51778-C2-1-R, cofinanced by the European Regional Development Fund) and SUPERINKS project (RTC-2015-3640-3, cofinanced by the European Regional Development Fund). We also thank support from the European Union for EUROTAPES project (FP7-NMP-Large-2011-280432) and ULTRASUPERTAPE project (H2020 ERC-2014-ADG-669504) and from the Catalan Government with 2014-SGR-753 and Xarmae. The authors acknowledge the technical support of Servei de Microscópia, and Servei de Difracció de Raigs- X, all at the UAB, and Dr Judith Oró (Microscope Service) at the ICMAB-CSIC, Dr Guillaume Sauthier for his support in XPS analysis. NCG acknowledge the PIF predoctoral fellowship from the Universitat Autònoma de Barcelona.

References

1 M. Segev-Bar and H. Haick, *ACS Nano*, 2013, **7**, 8366–8378.
2 L. E. Woodard, C. L. Dennis, J. A. Borchers, A. Attaluri, E. Velarde, C. Dawidczyk, P. C. Searson, M. G. Pomper and R. Ivkov, *Sci. Rep.*, 2018, **8**, 1–13.
3 M. Mahmoudi, M. Yu, V. Serpooshan, J. C. Wu, R. Langer, R. T. Lee, J. M. Karp and O. C. Farokhzad, *Nat. Nanotechnol.*, 2017, **12**, 845–855.
4 S. A. Bonke, A. M. Bond, L. Spiccia and A. N. Simonov, *J. Am. Chem. Soc.*, 2016, **138**, 16095–16104.

5 Q. Jia, S. Ghoshal, J. Li, W. Liang, G. Meng, H. Che, S. Zhang, Z. F. Ma and S. Mukerjee, *J. Am. Chem. Soc.*, 2017, **139**, 7893–7903.
6 A. Noori, M. F. El-Kady, M. S. Rahmanifar, R. B. Kaner and M. F. Mousavi, *Chem. Soc. Rev.*, 2019, **48**, 1272–1341.
7 R. R. Salunkhe, Y. V. Kaneti and Y. Yamauchi, *ACS Nano*, 2017, **11**, 5293–5308.
8 M. E. Franke, T. J. Koplin and U. Simon, *Small*, 2006, **2**, 36–50.
9 S. Han, X. Liu, Y. Liu, Z. Xu, Y. Li, M. Hong, J. Luo and Z. Sun, *J. Am. Chem. Soc.*, 2019, **141**, 12470–12474.
10 B.-W. Li, M. Osada, Y.-H. Kim, Y. Ebina, K. Akatsuka and T. Sasaki, *J. Am. Chem. Soc.*, 2017, **139**, 10868–10874.
11 T. Li, Y. Pan, Z. Wang, Y. Xia, Y. Chen and W. Huang, *J. Mater. Chem. A*, 2017, **5**, 12602–12652.
12 M. Niederberger, G. Garnweitner, N. Pinna and M. Antonietti, *J. Am. Chem. Soc.*, 2004, **126**, 9120–9126.
13 M. B. Smith, K. Page, T. Siegrist and A. Et, *J. Am. Chem. Soc.*, 2008, **130**, 6955–6963.
14 D. Caruntu, T. Rostamzadeh, T. Costanzo, S. Salemizadeh Parizi and G. Caruntu, *Nanoscale*, 2015, **7**, 12955–12969.
15 S. O'Brien, L. Brus and C. B. Murray, *J. Am. Chem. Soc.*, 2001, **123**, 12085–12086.
16 K. De Keukeleere, J. Feys, M. Meire, J. De Roo, K. De Buysser, P. Lommens and I. Van Driessche, *J. Nanopart. Res.*, 2013, **15**, 2074.
17 J. De Roo, K. De Keukeleere, J. Feys, P. Lommens, Z. Hens and I. Van Driessche, *J. Nanopart. Res.*, 2013, **15**, 1778.
18 Z. Lu, Y. Tang, L. Chen and Y. Li, *J. Cryst. Growth*, 2004, **266**, 539–544.
19 J. Liu and J. C. Berg, *J. Mater. Chem.*, 2007, **17**, 4430–4435.
20 C. N. Chervin, B. J. Clapsaddle, H. W. Chiu, A. E. Gash, J. H. Satcher and S. M. Kauzlarich, *Chem. Mater.*, 2006, **18**, 1928–1937.
21 A. E. Danks, S. R. Hall and Z. Schnepp, *Mater. Horiz.*, 2016, **3**, 91–112.
22 D. Gömpel, M. N. Tahir, M. Panthöfer, E. Mugnaioli, R. Brandscheid, U. Kolb and W. Tremel, *J. Mater. Chem. A*, 2014, **2**, 8033–8040.
23 M. Niederberger and G. Garnweitner, *Chem. - Eur. J.*, 2006, **12**, 7282–7302.
24 I. Bilecka and M. Niederberger, *Nanoscale*, 2010, **2**, 1358–1374.
25 I. Bilecka, L. Luo, I. Djerdj, M. D. Rossell, M. Jagodič, Z. Jagličić, Y. Masubuchi, S. Kikkawa and M. Niederberger, *J. Phys. Chem. C*, 2011, **115**, 1484–1495.
26 K. De Keukeleere, J. De Roo, P. Lommens, J. C. Martins, P. Van Der Voort and I. Van Driessche, *Inorg. Chem.*, 2015, **54**, 3469–3476.
27 M. Niederberger, *Acc. Chem. Res.*, 2007, **40**, 793–800.
28 N. Pinna, *J. Mater. Chem.*, 2007, **17**, 2769–2774.
29 N. Pinna, G. Garnweitner, M. Antonietti and M. Niederberger, *J. Am. Chem. Soc.*, 2005, **127**, 5608–5612.
30 Z. Li, M. Coll, B. Mundet, N. Chamorro, F. Vallès, A. Palau, J. Gazquez, S. Ricart, T. Puig and X. Obradors, *Sci. Rep.*, 2019, **9**, 1–14.
31 X. Obradors, T. Puig, Z. Li, C. Pop, B. Mundet, N. Chamorro, F. Vallés, M. Coll, S. Ricart, B. Vallejo, F. Pino, A. Palau, J. Gázquez, J. Ros and A. Usoskin, *Supercond. Sci. Technol.*, 2018, **31**, 044001.
32 L. Soler, J. Jareño, J. Banchewski, S. Rasi, N. Chamorro, R. Guzman, R. Yáñez, C. Mocuta, S. Ricart, J. Farjas, P. Roura-Grabulosa, X. Obradors and T. Puig, *Nat. Commun.*, 2020, **11**, 344.
33 E. Solano, L. Perez-Mirabet, F. Martinez-Julian, R. Guzmán, J. Arbiol, T. Puig, X. Obradors, R. Yañez, A. Pomar, S. Ricart and J. Ros, *J. Nanopart. Res.*, 2012, **14**, 1034.
34 M. Han, Y. Rong, Q. Li, X. Xing and L. Kang, *CrystEngComm*, 2015, **17**, 1944–1951.
35 T. Charoonsuk, W. Vittayakorn, N. Vittayakorn, P. Seeharaj and S. Maensiri, *Ceram. Int.*, 2015, **41**, S87–S94.
36 M. L. Moreira, J. Andrés, V. R. Mastelaro, J. A. Varela and E. Longo, *CrystEngComm*, 2011, **13**, 5818–5824.
37 H. W. Lee, S. Moon, C. H. Choi and D. K. Kim, *J. Am. Ceram. Soc.*, 2012, **95**, 2429–2434.
38 K. Kanie, Y. Seino, M. Matsubara, M. Nakaya and A. Muramatsu, *New J. Chem.*, 2014, **38**, 3548–3555.
39 R. Mouta, R. X. Silva and C. W. A. Paschoal, *Acta Crystallogr., Sect. B: Struct. Sci., Cryst. Eng. Mater.*, 2013, **69**, 439–445.
40 C. J. Bartel, C. Sutton, B. R. Goldsmith, R. Ouyang, C. B. Musgrave, L. M. Ghiringhelli and M. Scheffler, *Sci. Adv.*, 2019, **5**, 1–10.
41 R. D. Shannon, *Acta Crystallogr., Sect. B: Struct. Sci., Cryst. Eng. Mater. A*, 1976, **32**, 751–767.
42 H. Hayashi, T. Nakamura and T. Ebina, *J. Phys. Chem. Solids*, 2013, **74**, 957–962.
43 G. Yang, Z. Yue, T. Sun, J. Zhao, Z. Yang and L. Li, *Appl. Phys. A*, 2008, **91**, 119–125.
44 J. Van Embden, A. S. R. Chesman and J. J. Jasieniak, *Chem. Mater.*, 2015, **27**, 2246–2285.
45 U. Schubert and N. Hüsing, *Synthesis of Inorganic Materials*, VCH-Wiley Verlag GmbH, Weinheim, 3rd edn, 2012.
46 N. Y. Turova, E. P. Turevskaya, V. G. Kessler and M. I. Yanovskaya, *The chemistry of Metal Alkoxide*, Kluwe Academi Publisher, 2002.
47 J. Martínez-Esaín, J. Faraudo, T. Puig, X. Obradors, J. Ros, S. Ricart and R. Yáñez, *J. Am. Chem. Soc.*, 2018, **140**, 2127–2134.
48 A. Vioux, *Chem. Mater.*, 1997, **9**, 2292–2299.
49 D. C. Bradley, *Chem. Rev.*, 2002, **89**, 1317–1322.
50 N. Y. Turova, E. P. Turevskaya, V. G. Kessler and M. I. Yanovskaya, Hydrolysis of Metal Alkoxides and Synthesis of Simple Oxides by The Sol-Gel Method, in *The Chemistry of Metal Alkoxides*, Springer, Boston, MA, 2002.
51 R. R. J. P. Corriu and D. Leclercq, *Angew. Chem., Int. Ed. Engl.*, 1996, **35**, 1420–1436.
52 J. Owen, *Science*, 2015, **347**, 615–616.
53 M. A. Boles, D. Ling, T. Hyeon and D. V. Talapin, *Nat. Mater.*, 2016, **15**, 364.
54 U. Schubert, E. Arpac, W. Glaubitt, A. Helmerich and C. Chau, *Chem. Mater.*, 1992, **4**, 291–295.
55 A. Kumar, S. De, A. G. Samuelson and E. D. Jemmis, *Organometallics*, 2008, **27**, 955–960.

